RSC Advances

ROYAL SOCIETY OF CHEMISTRY

www.rsc.org/advances

Journal Name

ARTICLE

Synthesis, Crystal Structure and Physical Properties of FeV_4S_8 and $KFe_2V_8S_{16}$†

Received 00th January 20xx,
Accepted 00th January 20xx

DOI: 10.1039/x0xx00000x

www.rsc.org/

Lifang Sui,[a,b] Xian Zhang,[c] Zhangliu Tian,[b] Rongtie Huang, [a,b] Hui Zhang*[b], Jinjong Cheng,[a] Fuqiang Huang*[b,c]

Two compounds with the formulae of FeV_4S_8 and $KFe_2V_8S_{16}$ were successfully synthesized *via* melting salt method. The FeV_4S_8 crystallizes in the defective NiAs-like structure type of a monoclinic *I* 2/m space group, while the $KFe_2V_8S_{16}$ belongs to the pseudo-hollandite chalcogenide family and crystallizes in a monoclinic *C* 2/m space group. The structure of the FeV_4S_8 is composed of $[V_4S_8]^{3-}$ layers which are connected by $[FeS_6]^{9-}$ octahedra to form a 3D extended framework. The structure of $KFe_2V_8S_{16}$ is composed of a $[Fe_2V_8S_{16}]^-$ one-dimensional (1D) tunnel-type framework, where the Fe atoms partially occupies the V1 site. In the $KFe_2V_8S_{16}$ compound, the K^+ ions reside in the tunnels. Magnetic measurements show that the two compounds are both paramagnetic at high temperature. Weak ferromagnetic contributions are observed at low temperature for both the two compounds. The resistivity of FeV_4S_8 is measured to be 5.1×10^{-2} Ω·cm at room temperature. With the decrease of temperature, the compound shows clear metal-to-insulator phase transition at 163 K.

Introduction

Transition metal chalcogenides have aroused more and more interest for their various structures and abundant physical properties including thermoelectricity,[1-3] magnetoresistance[4-6], superconductivity,[7] as well as their potential applications in photovoltaics,[8] battery electrodes,[9] and catalysts.[10] Many of the transition metal chalcognides have a NiAs-type or metal deficient NiAs-type structure.[11-13] For instance, the VS compound belongs to the NiAs structure type with the space group of *P* 6_3/mmc (**Figure 1a**).[14] The V sites in the VS structure can be partially replaced by vacancies (□) to produce the metal deficient NiAs-type structures ($V_{1-x}S$). There are a series of vanadium sulfides including V_7S_8 (*x* = 1/8, **Figure 1b**),[15] V_3S_4 (*x* = 1/4, **Figure 1c**),[16] V_5S_8 (*x* = 3/8, **Figure 1e**),[17] and VS_2 (*x* = 1/2, **Figure 1g**).[18]

These vanadium sulfides are very interesting due to their various physical properties.[19-21] It is believed that the 3*d*-electrons, which vary widely, ranging from itineration to localization, are responsible for the metallic conductivity and magnetism of these compounds.[12, 22] Besides, the localization of the 3*d* electrons can be changed by varying the composition.[22] Therefore, varying the compositions and 3*d*-electon configurations are of scientific significance not only for exploring new materials with unique physical properties, but also for understanding the electron correlations in these narrow band metals. In addition, the physical properties of this type of materials can be further tuned by intercalating other metal ions into the defective sites in the metal deficient NiAs-type structure.[23, 24] There exist the $A_xV_5Q_8$ (*A* = alkali metal, alkaline-earth metal, and Tl; *Q* = S, Se, Te) which belongs to the pseudo-hollandite chalcogenide family.[25, 26] The structure is composed of a V_5Q_8 one-dimensional (1D) tunnel-type framework and *A* ions located in the tunnels (**Figure 1f**). The intercalated A ions act as electron donors which also can change the 3*d*-electon configurations, hence they could lead to fantastic transport and magnetic properties.[27, 28] Furthermore, the substitution of the V sites in the pseudo-hollandite chalcogenides by other transition metal ions is an easy way to change the 3*d*-electron configurations. Besides, it is believed that the introduction of other components can lead to the formation of structural/functional units, which is beneficial for multi-functional device applications.[29-32]

[a] Department of Material Sciences and Engineering, Shanghai University, Shanghai 200444, P.R. China.
[b] CAS Key Laboratory of Materials for Energy Conversion and State Key Laboratory of High Performance Ceramics and Superfine Microstructures, Shanghai Institute of Ceramics, Chinese Academy of Sciences, Shanghai 200050, P. R. China. E-mail: huangfq@mail.sic.ac.cn.
[c] Beijing National Laboratory for Molecular Sciences, College of Chemistry and Molecular Engineering, Peking University, Beijing 100871, P. R. China..

† Footnotes relating to the title and/or authors should appear here.
Electronic Supplementary Information (ESI) available: The $[V_4S_8]^{3-}$ layers in FeV_4S_8 and $[V_8S_{16}]^{7-}$ layers in $KFe_2V_8S_{16}$ crystal structures. M-T curves of FeV_4S_8 single crystals measured at different magnetic field. See DOI: 10.1039/x0xx00000x

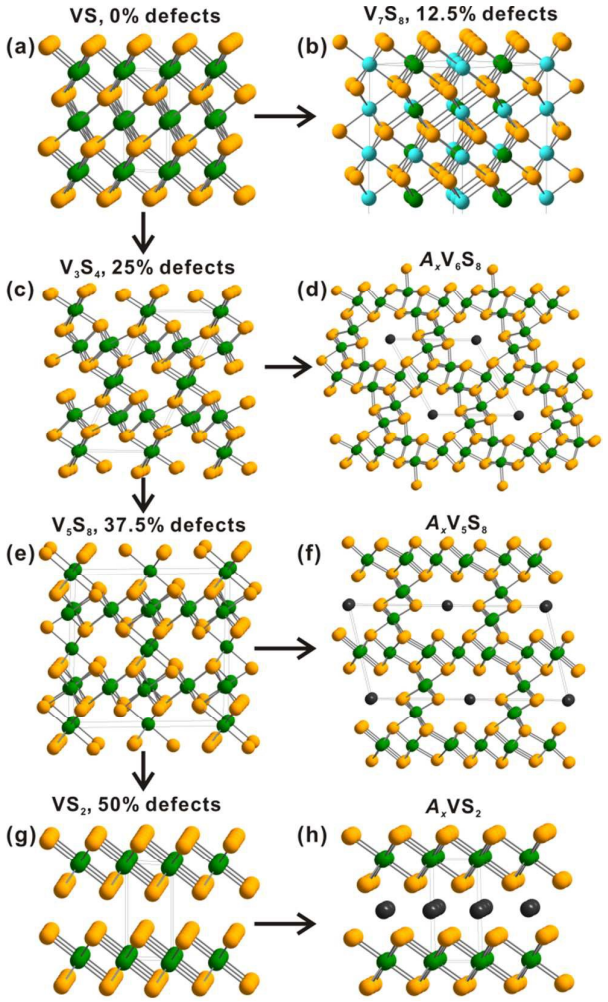

Figure 1. Crystal structures of NiAs and defective NiAs. (a) VS. (b) V_7S_8, only half of the unit cell is shown. The V sites with 75% occupation are highlighted by blue. (c) V_3S_4. (d) $A_xV_6S_8$. (e) V_5S_8. (f) $A_xV_5S_8$. (g) VS_2. (h) A_xVS_2

Hence, in this work, we presented two new sulfides FeV_4S_8 and $KFe_2V_8S_{16}$, which were synthesized by melting salt method. The FeV_4S_8 compound, which belongs to the defective NiAs-type structure, crystalizes in a monoclinic *I* 2/m space group. The $KFe_2V_8S_{16}$ compound belongs to the pseudo-hollandite chalcogenides family, whose structure is composed of a $[Fe_2V_8S_{16}]^-$ one-dimensional (1D) tunnel-type framework and K^+ ions residing in the tunnels. However, the variation of compositions and intercalation of different transition or alkali metal ions into the valium sulfides not only induce the structure change from V_5S_8 but also significantly change the 3d configurations, leading to the variation of their physical properties. Both the FeV_4S_8 and $KFe_2V_8S_{16}$ compounds show Curie-Weiss behavior at high temperature and weak ferromagnetic ordering at low temperature. Temperature dependent resistivity measurements indicate that the FeV_4S_8 compound is a metal at room temperature. A metal-to-insulator transition occurred at 163 K. The physical properties of the two compounds are quite different from the parent compound V_5S_8. Therefore, the syntheses of the two new compounds are important for basic research in this area.

Experimental

Synthesis of FeV_4S_8 and $KFe_2V_8S_{16}$ Single Crystals.

Single crystals of $KFe_2V_8S_{16}$ were prepared *via* melting salt method. Starting materials of K_2S powder (99.7%, Alfa), Fe powder (99.98%, Alfa), V powder (99.9% Alfa), S powder (99.5%, SCRC), and KI powder (99%, SCRC) were used without further treatment. To synthesize the $KFe_2V_8S_{16}$ single crystals, a starting material of K_2S, Fe, V, S, and KI were grounded uniformly in the molar ratio of 1:4:16:32:100. Then the mixture was loaded into a silica tube, followed by flame-sealing under vacuum (10^{-3} mbar). The tube was slowly heated to 1073 K, and was held at this temperature for 3 days. Afterwards, the tube was slowly cooled to 873 K at the ratio of 3 K/h. Finally, the furnace was turned off to cool the tube to room temperature. The melt was washed and sonicated by water for several times, and the obtained black crystals were dried by acetone. To synthesize the FeV_4S_8 single crystals, similar procedure was performed, while the molar ratio of starting material of Fe, V, S, and KI was 4:16:32:100.

Single Crystal X-ray Diffraction.

Suitable crystals were chosen to perform the data collections. Single crystal X-ray diffraction was performed on a Bruker D8QUEST diffractometer equipped with Mo K_α radiation. The diffraction data were collected at room temperature by the ω- and φ-scan methods. The crystal structures were solved and refined using APEX2 program.[33] Absorption corrections were performed using the multi-scan method (SADABS).[34] The detailed crystal data and structure refinement parameters are summarized in **Table 1.** Selected bond lengths are summarized in **Table 2.**

Table 1. Crystal data and structure refinement parameters for FeV_4S_8 and $KFe_2V_8S_{16}$ crystal.

formula	FeV_4S_8	$KFe_2V_8S_{16}$		
F_w (g/mol)	516.09	1071.28		
T (K)	293(2)	295(2)		
λ (Å)	0.71073	0.71073		
Crystal system	monoclinic	monoclinic		
Space group	*I* 2/m	*C* 2/m		
a (Å)	7.9000(11)	17.465(5)		
b (Å)	6.6425(11)	3.293(1)		
c (Å)	8.0327(11)	8.473(3)		
α (deg.)	90	90		
β (deg.)	91.202(5)	103.82(1)		
γ (deg.)	90	90		
V (Å^3)	421.43(11)	473.2(3)		
Z	2	1		
ρ (g/cm^3)			4.067	3.759
μ (mm^{-1})			67.221	7.215
F(000)			492	511

***R*(int)**	0.0507	0.0245	
Refinement method		Full-matrix least-squares on F^2	
***R* ($I > 2\sigma(I)$)**		0.0308	0.0161
***wR*^{2} (all data)**		0.0642	0.0423
GOF		1.074	1.102

Table 2. Selected bond distancess of FeV_4S_8 and $KFe_2V_8S_{16}$.

FeV_4S_8		$KFe_2V_8S_{16}$	
Fe(1)-S(2)	2.3678	**V(1)|Fe1-S(1)**	2.2795
Fe(1)-S(3)	2.4055	**V(1)|Fe1-S(1)**	2.3331
Fe(2)-S(1)	2.2824	**V(1)|Fe1-S(4)**	2.5079
Fe(2)-S(2)	2.2995	**V(1)|Fe1-S(3)**	2.5119
Fe(2)-S(3)	2.481	**V(2)-S(3)**	2.3819
V(1)-S(1)	2.3119	**V(2)-S(2)**	2.4005
V(1)-S(2)	2.3771	**V(3)-S(3)**	2.2897
V(1)-S(3)	2.4447	**V(3)-S(2)**	2.3136
V(2)-S(1)	2.3116	**V(3)-S(4)**	2.4812
V(2)-S(2)	2.3699 /2.4065		
V(2)-S(3)	2.4267		

Characterization.

The obtained crystals were investigated with a JEOL (JSM6510) scanning electron microscope equipped by energy dispersive X-ray spectroscopy (EDXS, Oxford Instruments). Powder X-ray diffraction of the FeV_4S_8 samples were collected on a Bruker D8QUEST diffractometer equipped with mirror-monochromated Mo K_α radiation.

Physical Property Measurements.

For resistivity measurement the compact sample was obtained by sintering polycrystalline pellet at 500 °C for 20 h in vacuumed silica tube. The temperature dependence of the resistivity was measured using the standard four-probe technique by the ETO model on the Physical Property Measurement System (PPMS, Quantum Design, DynaCOOL). The temperature dependence of magnetization was measured both under zero-field-cooled (ZFC) and field-cooled (FC) models in magnetic fields of 1000 Oe, 5000 Oe and 10000 Oe from 2K to 300 K on PPMS. The field dependence of magnetization was measured at 2 K, 10K, and 300 K under the applied magnetic field from −2 T to 2 T.

Results and discussion

Synthesis and Crystal Structure Description.

Melting salt method is a good way to grow well defined single crystals at relatively low temperature. The SEM of the as-synthesized FeV_4S_8 and $KFe_2V_8S_{16}$ single crystals are shown in **Figure 2a & 2c.** In order to check the homogeneity of their compositions, elemental analyses of the crystals were performed (**Figure 2b** & **2d**). The Fe/V/S ratio is 1/3.8/7.7, while the K/Fe/V/S ratio is 1/1.8/7.5/15.1.

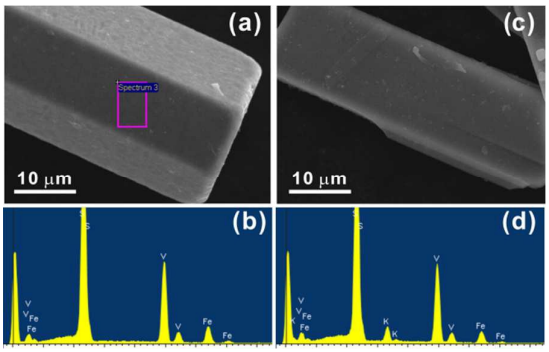

Figure 2. SEM images of the FeV_4S_8 (a) and $KFe_2V_8S_{16}$ (c) crystal. EDX spectra of the FeV_4S_8 (b) and $KFe_2V_8S_{16}$ (d) crystals.

The FeV_4S_8 compound, which belongs to the metal-deficient NiAs structure type, crystallizes in a monoclinic space group *I* 2/m (**Figure 3a**). FeV_4S_8 contains two independent Fe sites (2d, 4e), two independent V sites (4i and 4g), and three independent S sites (4i, 4i, and 8j). Both Fe and V locate in the octahedral coordination environments. The structure of FeV_4S_8 compound is constructed by $[V_4S_8]^{3-}$ layers (**Figure S1a in Supporting Information**) which are connected by $[FeS_6]^{9-}$ octahedra. The occupations of the two Fe sites are 89% (Fe1) and 11% (Fe2), respectively. Therefore, 37.5% octahedral sites remain unoccupied. The average distance of Fe-S is 2.3673(3) Å, while the Fe-S distance in the reported structures is 2.453 Å in FeS, and 2.277 Å in Ba_2FeS_3. The average V-S distance is 2.3799(3) Å, comparable to that in V_5S_8 (2.390 Å).

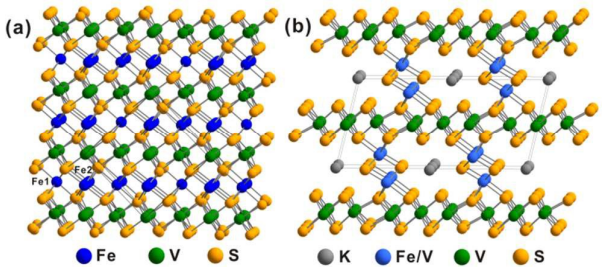

Figure 3. (a) Crystal structure of FeV_4S_8 view along the *b* axis. (b) Crystal structure of $KFe_2V_8S_{16}$ view along the *b* axis.

The $KFe_2V_8S_{16}$ has the similar structure with the pseudo-hollandite chalcogenide $K_xV_5S_8$ (**Figure 3b**). The structure of $KFe_2V_8S_{16}$ is composed of a $[Fe_2V_8S_{16}]^-$ one-dimensional (1D) tunnel-type framework and K^+ ions residing in the tunnels (**Figure 3b**). The structure contains three independent V sites (V1: 4i; V2: 2d; V3: 4i), in which the V1 site is half replaced by Fe atoms. The $[Fe_2V_8S_{16}]^-$ framework has the $[V_8S_{16}]^{7-}$ layers (**Figure S1b in Supporting Information**) which have similar structure with the $[V_4S_8]^{3-}$ layers in FeV_4S_8 compound. However, the $[V_8S_{16}]^{7-}$ layers are connected by $[Fe/VS_3]^{3-}$ double chains but not $[FeS_6]^{9-}$ octahedra. The average V–S distance is 2.360 Å, which is comparable to that in the

reported structure (2.40 Å in $K_xV_5S_8$). In addition, the average V1/Fe1–S bond length is 2.41 Å, slightly larger than the average distance of V–S (2.36 Å).

The valance state of the V1 atoms in the V_5S_8 is +3, while the average valance of the V2 and V3 is +3.25. From the point view of crystal structure, the average V1–S distance is 0.233 Å similar with the average distance of V2–S and V3–S. For the FeV_4S_8 compounds, the average Fe–S and V–S distances are 2.3673(3) Å and 2.3799(3) Å, respectively, indicating the similar radii of Fe and V ions. Therefore, we can assume the valance state of Fe ions is also +3 ($3d^5$ configuration).

Magnetic Properties.

Vanadium sulfides that belong to the defective NiAs type compounds are of significance due to their abundant physical properties, such as the itinerant antiferromagnetism, and considerably localization antiferromagnetism. It is reported that the VS and V_3S_4 show weak temperature-independent paramagnetism, whereas V_5S_8 shows Curie-Weiss behavior above the Neel temperature (T_N). In addition, the V_3S_4 and V_5S_8 order antiferromagnetically below T_N = 8 and 32 K. It is believed that the tunable physical properties of this series of vanadium sulfides are due to the change of 3d electron configurations. Therefore, further tuning the 3d electron configurations in this system may produce intriguing physical properties. The reasonable way to change the 3d electron configurations is intercalation of other 3d metal ions or alkali metal ions. The physical properties of the two compounds are quite different from the parent compound V_5S_8. By intercalation of Fe ions, the antiferromagnetic ordering disappear, while the weak ferromagnetic ordering shows up at low temperature.

Single crystals of FeV_4S_8 are picked manually for the magnetic susceptibility measurements. **Figure 3a** shows the zero-field cooled (ZFC) and field-cooled (FC) curves measured at the magnetic fields of 1000 Oe. Obviously, the FeV_4S_8 compound shows clear Curie-Weiss behavior in the whole temperature range. Curie-Weiss fitting of the magnetic susceptibility yields values of Curie constant *C* and Weiss constant ϑ are 0.16 emu·K·mol^{-1} and -2.1 K, respectively. The effective magnetic moments (μ_{eff}) can be evaluated from the following equation: $\mu_{eff} = \sqrt{8C}\mu_B$. The derived effective magnetic moments are 1.13 μ_B. The negative value of the Weiss constant indicates that there are weak ferromagnetic interactions at low temperature. Besides, by increasing external magnetic field, the temperature dependent magnetic susceptibility disobeys the Curie-Weiss law at low temperature (**Figure S2** in Supporting Information). In addition, separations between ZFC and FC curves are also observed at low temperature which can further confirm the existence of weak ferromagnetic contributions. The hysteresis loops of FeV_4S_8 compound are shown in **Figure 3b**. At high temperature, the *M-H* curves show linear dependence, which is consist with the paramagnetic behavior. However, the *M-H* curves bend slightly at 2 K, implying the weak ferromagnetic contributions. It is known that the V_5S_8 have an antiferromagnetic phase transition at 32 K, which is due to the itineration of 3*d* electrons. The absence of antiferromagnetic ordering might due to the random distribution of Fe atoms which break down the itineration of electrons.

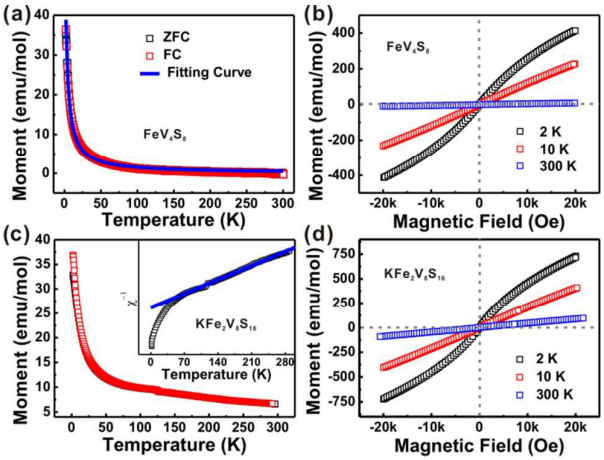

Figure 4. (a) Temperature-dependence of the magnetization of the FeV_4S_8 compound. (b) Magnetic hysteresis of the FeV_4S_8 compound at 2 K, 10 K and 300 K. (c) Temperature-dependence of the magnetization of the $KFe_2V_8S_{16}$ compound. Inset: The inverse magnetic susceptibility *vs.* temperature plot. The blue line is the linear fit of the magnetic susceptibility data from 300 K to 50 K. (d) Magnetic hysteresis of the $KFe_2V_8S_{16}$ compound at 2 K, 10 K and 300 K.

The temperature dependent magnetic susceptibility of $KFe_2V_8S_{16}$ is shown in **Figure 3c**. At high temperature, the $KFe_2V_8S_{16}$ compound also shows Curie-Weiss behavior. However, a separation of ZFC and FC shows up at low temperature, which indicates the presence of ferromagnetic interactions. The *M-H* curves of $KFe_2V_8S_{16}$ also bend slightly at 2 K, implying the weak ferromagnetic contributions. The high temperature susceptibility of $KFe_2V_8S_{16}$ is fitted to Curie-Weiss law (**Figure 3c** inset). The obtained *C* and θ is 3.9 emu·K·mol^{-1} and –295 K, respectively.

Electrical Transport Properties.

Phase purity of the FeV_4S_8 compact disk was checked by powder X-ray diffraction, as shown in **Figure 5a**. All the peaks can be indexed, indicating high degree of purity crystallinity. The electrical transport property of the FeV_4S_8 disk is depicted in **Figure 5b**. In the high temperature region, the resistivity decreases with the deceasing temperature, which indicates the metallic behavior of the FeV_4S_8 disk. The room temperature resistivity is 0.024 Ω·cm. The resistivity increases sharply at 163 K, which demonstrates the metal-to-insulator phase transition. Therefore, the substitution of V1 by Fe atoms significantly changes the electrical transport properties from the V_5S_8 which shows metallic conductivity in the whole temperature range (300~2 K). Besides V_5S_8, many other vanadium sulfides, including VS, V_3S_4, and VS_2, also show metallic behaviors. However, the FeV_4S_8 has a metal-to-

insulator phase transition around 163 K which is rare in this series of compounds. The magnetic resistances of the FeV_4S_8 are also measured under different external magnetic field **(Figure 5b & 5c)**. At low temperature, the FeV_4S_8 disk shows slightly negative magnetoresistance with ~0.9% of resistance reduction. However, the positive to negative transition in the magnetoresistance that occurred in V_5S_8 at 4.2 K is not observed in our case, indicating the absence of spin flopping transition.[35]

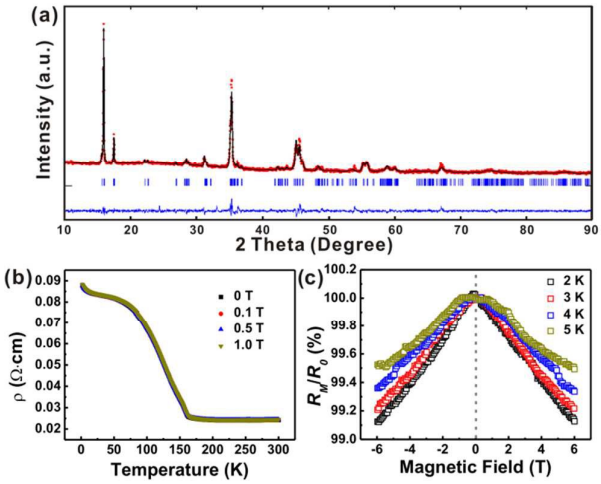

Figure 5. (a) Powder X-ray diffraction of the FeV_4S_8 disk. (b) Temperature-dependent resistivity of the FeV_4S_8 disk under different external magnetic field. (c) Magnetic field dependence of the magnetoresistance of the FeV_4S_8 disk.

Conclusions

In summary, we successfully synthesized two compounds, namely the FeV_4S_8 and $KFe_2V_8S_{16}$, *via* melting salt method. The FeV_4S_8 crystallizes in the defective NiAs-like structure type of a monoclinic *I* 2/m space group, while the $KFe_2V_8S_{16}$ belongs to the pseudo-hollandite chalcogenide family. The structure of FeV_4S_8 features 3D extended framework, which is composed of $[V_4S_8]^{3-}$ layers and $[FeS_6]^{9-}$ octahedra. The structure of $KFe_2V_8S_{16}$ is composed of a $[Fe_2V_8S_{16}]^{-}$ one-dimensional (1D) tunnel-type framework. Different from the FeV_4S_8 framework, the $[Fe_2V_8S_{16}]^{-}$ in $KFe_2V_8S_{16}$ is composed of $[V_8S_{16}]^{7-}$ layers and $[Fe/VS_3]^{3-}$ double chains. The two compounds are both paramagnetic at high temperature, and possess weak ferromagnetic contribution at low temperature. Electrical transport and magnetoresistance properties of the FeV_4S_8 were investigated with the room temperature resistivity of 5.1×10^{-2} Ω·cm. Besides, The FeV_4S_8 compound also shows clear metal-to-insulator phase transition at 163 K.

Acknowledgements

This work was financially supported by Innovation Program of the CAS (Grant KJCX2-EW-W11), "Strategic Priority Research Program (B)" of the Chinese Academy of Sciences (Grants XDB04040200), NSF of China (Grants 91122034, 51125006, 51202279, 61376056, 21201012, 51402341 and 51402335).

Notes and references

1 G. Chen, M. S. Dresselhaus, G. Dresselhaus, J. P. Fleurial and T. Caillat, *Int. Mater. Rev.*, 2003, **48**, 45-66.
2 G. D. Mahan, *J. Appl. Phys.*, 1989, **65**, 1578-1583.
3 G. J. Snyder and E. S. Toberer, *Nat. Mater.*, 2008, **7**, 105-114.
4 R. Xu, A. Husmann, T. F. Rosenbaum, M. L. Saboungi, J. E. Enderby and P. B. Littlewood, *Nature*, 1997, **390**, 57-60.
5 Y. Q. Guo, J. Dai, J. Y. Zhao, C. Z. Wu, D. Q. Li, L. D. Zhang, W. Ning, M. L. Tian, X. C. Zeng and Y. Xie, *Phys. Rev. Lett.*, 2014, **113**.
6 T. Block and W. Tremel, *J. Alloy Compd.*, 2006, **422**, 12-15.
7 J. D. Weiss, C. Tarantini, J. Jiang, F. Kametani, A. A. Polyanskii, D. C. Larbalestier and E. E. Hellstrom, *Nat. Mater.*, 2012, **11**, 682-685.
8 S. E. Habas, H. A. S. Platt, M. F. A. M. van Hest and D. S. Ginley, *Chem. Rev.*, 2010, **110**, 6571-6594.
9 Y. H. Liao, K. S. Park, P. H. Xiao, G. Henkelman, W. S. Li and J. B. Goodenough, *Chem. Mater.*, 2013, **25**, 1699-1705.
10 V. Iliev, L. Prahov, L. Bilyarska, H. Fischer, G. Schulz-Ekloff, D. Wohrle and L. Petrov, *J. Mol. Catal. A-Chem.*, 2000, **151**, 161-169.
11 K. Motizuki, *J. Magn. Magn. Mater.*, 1987, **70**, 1-7.
12 S. P. Farrell and M. E. Fleet, *Phys. Chem. Miner.*, 2001, **28**, 17-27.
13 M. Y. C. Teo, S. A. Kulinich, O. A. Plaksin and A. L. Zhu, *J. Phys. Chem. A*, 2010, **114**, 4173-4180.
14 M. Knecht, H. Ebert and W. Bensch, *J. Alloy Compd.*, 1997, **246**, 166-176.
15 S. Brunie, Chevreto.M and Kauffman.Jm, *Mater. Res. Bull.*, 1972, **7**, 253-&.
16 I. Kawada, M. Nakanoonoda, M. Ishii, M. Saeki and M. Nakahira, *J. Solid State Chem.*, 1975, **15**, 246-252.
17 I. Kawada, M. Nakanoonoda, M. Ishii and M. Saeki, *Acta Crystallogr. A*, 1975, **31**, S68-S68.
18 K. Friese, O. Jarchow and K. Kato, *Z. Kristallogr.*, 1997, **212**, 648-655.
19 S. Funahashi, H. Nozaki and I. Kawada, *J. Phys. Chem. Solids*, 1981, **42**, 1009-1013.
20 A. Fujimori, M. Saeki and H. Nozaki, *Phys. Rev. B*, 1991, **44**, 163-169.
21 Y. Kitaoka and H. Yasuoka, *J. Phys. Soc. Jpn.*, 1980, **48**, 1949-1956.
22 A. Muller, R. Sessoli, E. Krickemeyer, H. Bogge, J. Meyer, D. Gatteschi, L. Pardi, J. Westphal, K. Hovemeier, R. Rohlfing, J. Doring, F. Hellweg, C. Beugholt and M. Schmidtmann, *Inorg. Chem.*, 1997, **36**, 5239-5250.
23 Y. Sahoo and A. K. Rastogi, *Physica B*, 1995, **215**, 233-242.
24 M. A. Ruman and A. K. Rastogi, *J. Phys. Chem. Solids*, 2003, **64**, 77-85.
25 S. Petricek, H. Boller and K. O. Klepp, *Solid State Ionics*, 1995, **81**, 183-188.
26 K. D. Bronsema, R. Jansen and G. A. Wiegers, *Mater. Res. Bull.*, 1984, **19**, 555-562.
27 W. Bensch and E. Worner, *Solid State Ionics*, 1992, **58**, 275-283.
28 W. Bensch, E. Worner, M. Muhler and U. Ruschewitz, *Eur. J. Sol. State Inorg.*, 1993, **30**, 645-658.
29 X. Zhang, J. He, W. Chen, K. Zhang, C. Zheng, J. Sun, F. Liao, J. Lin and F. Huang *Chem. Eur. J.*, 2014, **20**, 5977-5982.
30 X. Zhang, W. Chen, D. J. Mei, C. Zheng, F. H. Liao, Y. T. Li, J. H. Lin and F. Q. Huang, *J. Alloys Compd.*, 2014, **610**, 671-675.

31 X. Zhang, Q. Wang, Z. Ma, J. He, Z. Wang, C. Zheng, J. Lin and F. Huang, *Inorg. Chem.*, 2015, **54**, 5301-5308.
32 S. Meng, X. Zhang, G. H. Zhang, Y. M. Wang, H. Zhang and F. Q. Huang, *Inorg. Chem.*, 2015, **54**, 5768-5773.
33 B. Optics, *Chem. Eng. News*, 2014, 16-16.
34 A. B. Bruker, *Zh. Obshch. Khim.*, 1957, **27**, 2593-2598.
35 H. Nozaki and Y. Ishizawa, *Phys. Lett. A*, 1977, **63**, 131-132.